INTERNATIONAL JOURNAL FOR NUMERICAL METHODS IN FLUIDS, VOL. 2, 349–366 (1982)

FINITE ELEMENT, STREAM FUNCTION–VORTICITY SOLUTION OF STEADY LAMINAR NATURAL CONVECTION

W. N. R. STEVENS*

Department of Electrical and Electronic Engineering, University of Nottingham, U.K.

SUMMARY

Stream function–vorticity finite element solution of two-dimensional incompressible viscous flow and natural convection is considered. Steady state solutions of the natural convection problem have been obtained for a wide range of the two independent parameters. Use of boundary vorticity formulae or iterative satisfaction of the no-slip boundary condition is avoided by application of the finite element discretization and a displacement of the appropriate discrete equations. Solution is obtained by Newton–Raphson iteration of all equations simultaneously. The method then appears to give a steady solution whenever the flow is physically steady, but it does not give a steady solution when the flow is physically unsteady. In particular, no form of asymmetric differencing is required. The method offers a degree of economy over primitive variable formulations. Physical results are given for the square cavity convection problem. The paper also reports on earlier work in which the most commonly used boundary vorticity formula was found not to satisfy the no-slip condition, and in which segregated solution procedures were attempted with very minimal success.

KEY WORDS Viscous Flow Modelling Convection Modelling Flow Boundary Treatment

1. INTRODUCTION

Most finite difference studies of incompressible viscous flow and convection in two dimensions have used the stream function–vorticity formulation. This formulation has the advantage of satisfying mass conservation exactly and reducing the number of simultaneous partial differential equations by one (from three to two for uncoupled viscous flow alone). With the finite element method however the majority of studies have used the primitive variable approach. In one of the first finite element works Taylor and Hood[1,2] examined both forms of approach, but dropped stream function–vorticity in favour of primitive variables. Primitive variables were also chosen by Oden and Wellford,[3] and then by Kawahara *et al.*[4] and Gartling and Becker[5] amongst others. Stream function–vorticity was chosen in the early works of Cheng[6] and Baker.[7]

The difficulty with the stream function–vorticity approach is that, of two second order partial differential equations, one, a Poisson equation for stream function, has two boundary conditions instead of the one required, and the other, the vorticity transport equation, has no boundary condition. Finite difference workers have for long met this difficulty by defining boundary vorticity from the variation along the boundary normal of the stream function field determined in a previous iteration. We shall call this the boundary vorticity formula method.

---

* Present address: PAFEC Ltd., Strelley Hall, Nottingham, U.K.

0271–2091/82/040349–18$01.80

Received 25 November 1980
Revised 22 January 1982

Finite element workers who have adopted the stream function–vorticity formulation have followed the same procedure. This is unfortunate because the effect of the boundary vorticity formulae appears to be highly dubious: this is discussed further in Section 3 of this paper. Further it happens that the finite element discretization naturally allows the difficulty to be avoided. This fact was apparently first pointed out in the literature by Campion-Renson and Crochet,[8] and is also illustrated further in this paper. The difficulty can also be avoided by combining the two equations to give one fourth order equation. This idea has been exploited by Olson and Tuann,[9] who use plate bending elements and call the method simply the stream function approach.

This paper describes the modelling of natural convection using the stream function–vorticity formulation and the finite element method and avoiding the boundary vorticity difficulty. For natural convection, in addition to the viscous flow equations which the above cited references have been concerned with, there is a further second order equation for the transport of heat. The heat transport in turn drives the flow through buoyancy. Previous finite element studies of natural convection through primitive variables have included the work of Gartling,[10] Kawahara *et al.*,[4] Taylor and Ijam,[11] Young *et al.*,[12] Piva and DiCarlo[13] and Zienkiewicz *et al.*[14] The stream function–vorticity approach has previously been adopted in a finite element context at low Rayleigh numbers by Tabarrok and Lin.[15]

Methods of solution of the coupled partial differential equations can be broadly divided into two categories: segregated approaches, where each equation is solved in rotation with some form of relaxation of variable values in the loop, and the simultaneous approach where a Jacobian involving all equations and all variables can be formed. The general attraction of the segregated approaches is the smaller storage requirement. Following the paper of Tabarrok and Lin,[15] and because the most available computer was a minicomputer of rather limited storage at the time, this author originally attempted segregated approaches. Success was minimal, but because the experience may bear upon attempts that other workers might make, the results are briefly described in Section 3 of this paper. This section also contains a brief discussion of the boundary vorticity formula method which was adopted initially. In contrast to the segregated approach, the simultaneous approach with the Newton–Raphson method and avoidance of the boundary vorticity difficulty worked very well. The formulation is therefore given first in Section 2 as applied with this method. The implementation of the method, computational questions, and results on the performance of the method are given in Section 4. The physical results are given and discussed in Section 5.

2. FORMULATION

The derivation of the stream function–vorticity formulation from the primitive equations for transport of momentum and energy and for continuity under the incompressible assumption will not be repeated here since it is given in many other places. If non-dimensional temperature, co-ordinates, and time scale are defined by

$$\theta = \frac{T - T_c}{T_h - T_c}$$

$$X = \frac{x}{d}, \qquad Y = \frac{y}{d} \tag{1}$$

$$\tau = \frac{\alpha t}{d^2}$$

where T_h and T_c are suitable reference temperatures, d is a reference distance, and α is the fluid thermal diffusivity, then non-dimensional stream function and vorticity are

$$\Psi = \frac{\psi}{\alpha} \qquad \Omega = \frac{d^2\omega}{\alpha} \tag{2}$$

and the non-dimensional equations for natural convection under the usual Boussinesque approximation are

$$\frac{\partial\theta}{\partial\tau} = \nabla^2\theta - \left(\frac{\partial\Psi}{\partial Y}\frac{\partial\theta}{\partial X} - \frac{\partial\Psi}{\partial X}\frac{\partial\theta}{\partial Y}\right) \tag{3a}$$

$$\frac{1}{P}\frac{\partial\Omega}{\partial\tau} = \nabla^2\Omega - \frac{1}{P}\left(\frac{\partial\Psi}{\partial Y}\frac{\partial\Omega}{\partial X} - \frac{\partial\Psi}{\partial X}\frac{\partial\Omega}{\partial Y}\right) + R\frac{\partial\theta}{\partial X} \tag{3b}$$

$$0 = \nabla^2\Psi + \Omega \tag{3c}$$

where P and R are the fluid Prandtl number and the problem Rayleigh number:

$$P = \frac{\nu}{\alpha}$$

$$R = \frac{g\beta(T_h - T_c)d^3}{\nu\alpha}$$

where ν is the fluid kinematic viscosity (or viscous diffusivity), β is the fluid thermal expansion coefficient, and g is the acceleration due to gravity.

This non-dimensionalization is that suggested by de Vahl Davis *et al.*[16] for comparison of results of viscous flow computations. An alternative choice, to which we shall refer in Section 5, is to base the time scale on the viscous rather than the thermal diffusivity:

$$\tau_v = \frac{\nu}{d^2}t \tag{4}$$

The dimensionless velocity-related variables are then

$$\Psi_v = \frac{\psi}{\nu} = \frac{1}{P}\Psi, \qquad \Omega_v = \frac{d^2}{\nu}\omega = \frac{1}{P}\Omega \tag{5}$$

and equations (3) are replaced by

$$P\frac{\partial\theta}{\partial\tau_v} = \nabla^2\theta - P\left(\frac{\partial\Psi_v}{\partial Y}\frac{\partial\theta}{\partial X} - \frac{\partial\Psi_v}{\partial X}\frac{\partial\theta}{\partial Y}\right) \tag{6a}$$

$$\frac{\partial\Omega_v}{\partial\tau_v} = \nabla^2\Omega_v - \left(\frac{\partial\Psi_v}{\partial Y}\frac{\partial\Omega_v}{\partial X} - \frac{\partial\Psi_v}{\partial X}\frac{\partial\Omega_v}{\partial Y}\right) + G\frac{\partial\theta}{\partial X} \tag{6b}$$

$$0 = \nabla^2\psi_v + \Omega_v \tag{6c}$$

where G is the Grashoff number

$$G = \frac{g\beta(T_h - T_c)d^3}{\nu^2} = \frac{R}{P}$$

which is independent of the thermal diffusivity of the fluid.

The three dependent variables are expanded in the standard finite element way:

$$\Phi = \boldsymbol{\alpha}^{\mathrm{T}}\boldsymbol{\Phi} = \boldsymbol{\Phi}^{\mathrm{T}}\boldsymbol{\alpha}$$

where Φ stands for any of θ, Ω, or Ψ and $\boldsymbol{\alpha}$ is the vector of shape functions. The Galerkin discretization is then applied to equations (3), i.e. the equations are projected onto each of the shape functions. The terms in ∇^2 incorporate gradient type boundary conditions: Green's theorem gives

$$\langle \boldsymbol{\alpha}, \nabla^2 \boldsymbol{\alpha}^{\mathrm{T}} \rangle \boldsymbol{\Phi} = -\langle \nabla \boldsymbol{\alpha} \cdot \nabla \boldsymbol{\alpha}^{\mathrm{T}} \rangle \boldsymbol{\Phi} + \int_s \boldsymbol{\alpha} \frac{\partial \Phi}{\partial n} \, \mathrm{d}s \tag{7}$$

where the brackets denote integration over the problem region, the last integral is over the boundary, and $\mathbf{n}$ is the outward normal. For matrix rows for which the test function α_i pertains to a node which is not on the boundary the last term is zero. For rows for which the test function pertains to a node on a segment of boundary for which a gradient boundary condition applies, the prescribed gradient is substituted in the last term. For nodes on segments of boundaries where fixed value boundary conditions apply the appropriate equation of (7) becomes replaced as we discuss below. Equations (3) then give

$$\mathbf{M}\dot{\boldsymbol{\theta}} = -\mathbf{K}\boldsymbol{\theta} - \mathbf{a}(\boldsymbol{\Psi}, \boldsymbol{\theta}) + \mathbf{b}(\theta_n) \tag{8a}$$

$$\mathbf{M}\dot{\boldsymbol{\Omega}} = -PR\mathbf{K}\boldsymbol{\Omega} - \mathbf{a}(\boldsymbol{\Psi}, \boldsymbol{\Omega}) + PR\mathbf{C}\boldsymbol{\theta} + P\mathbf{b}(\Omega_n) \tag{8b}$$

$$0 = -\mathbf{K}\boldsymbol{\Psi} + \mathbf{M}\boldsymbol{\Omega} + \mathbf{b}(\Psi_n) \tag{8c}$$

where the volume integrals are

$$\mathbf{M} = \langle \boldsymbol{\alpha}, \boldsymbol{\alpha}^{\mathrm{T}} \rangle \tag{9a}$$

$$\mathbf{K} = \langle \nabla \boldsymbol{\alpha} \cdot \nabla \boldsymbol{\alpha}^{\mathrm{T}} \rangle \tag{9b}$$

$$\mathbf{C} = \langle \boldsymbol{\alpha}, \partial_x \boldsymbol{\alpha}^{\mathrm{T}} \rangle \tag{9c}$$

$$\mathbf{a}(\boldsymbol{\Psi}, \boldsymbol{\theta}) = \langle \boldsymbol{\alpha}, \partial_y \boldsymbol{\alpha}^{\mathrm{T}} \boldsymbol{\Psi}, \partial_x \boldsymbol{\alpha}^{\mathrm{T}} \boldsymbol{\theta} \rangle - \langle \boldsymbol{\alpha}, \partial_x \boldsymbol{\alpha}^{\mathrm{T}} \boldsymbol{\Psi}, \partial_y \boldsymbol{\alpha}^{\mathrm{T}} \boldsymbol{\theta} \rangle \tag{9d}$$

and $\mathbf{b}$ is the boundary integral

$$\mathbf{b}(\Phi_n) = \int_s \boldsymbol{\alpha} \partial_n \Phi \, \mathrm{d}s \tag{9e}$$

For the Newton–Raphson method, the left-hand sides of (8) are replaced by the negative of a set of residuals, $\mathbf{r}_\theta, \mathbf{r}_\Omega$, and $\mathbf{r}_\Psi$:

$$\mathbf{r}_\theta = \mathbf{K}\boldsymbol{\theta} + \mathbf{a}(\boldsymbol{\Psi}, \boldsymbol{\theta}) - \mathbf{b}(\theta_n) \tag{10a}$$

$$\mathbf{r}_\Omega = PR\mathbf{K}\boldsymbol{\Omega} + \mathbf{a}(\boldsymbol{\Psi}, \boldsymbol{\Omega}) - PR\mathbf{C}\boldsymbol{\theta} - P\mathbf{b}(\Omega_n) \tag{10b}$$

$$\mathbf{r}_\Psi = -\mathbf{M}\boldsymbol{\Omega} + \mathbf{K}\boldsymbol{\Psi} - \mathbf{b}(\Psi_n) \tag{10c}$$

We now discuss the application of the boundary conditions. First, the fixed value conditions. If node i is on such a segment of boundary for variable Φ, the residual $r_{\Phi,i}$ defined by (10) is deleted and replaced by,

$$r_{\Phi,i} = \Phi_i - \bar{\Phi}_i \tag{11}$$

$\bar{\Phi}_i$ being the prescribed value. This treatment applies to the prescribed temperature boundaries. It also applies to the constant stream function condition for an impermeable boundary, which means the entire boundary for natural convection in an enclosure.

Next, the gradient boundary conditions. For adiabatic segments of boundary the line integral $b_i(\theta_n)$ in the residual $r_{\theta,i}$, equations (10a) is zero. There remains the stream function gradient condition which occurs in this formulation in place of any condition on the vorticity. The appropriate residuals $r_{\Omega,i}$ are simply deleted and replaced by the residuals $r_{\Psi,i}$ which, as already noted are displaced by residuals of type (11). Thus the residuals $r_{\Psi,i}$ of type (10c) for boundary nodes are simply shifted in position in the system (and a change of sign is applied). For the no slip condition, the line integral $b_i(\Psi_n)$ is set to zero.

For the Newton–Raphson method, the iteration form is

$$\boldsymbol{\zeta}^{k+1} = \boldsymbol{\zeta}^k - \mathbf{J}^{-1}\mathbf{r}^k \tag{12}$$

k being the iteration count, where

$$\boldsymbol{\zeta} = (\boldsymbol{\theta}^{\mathrm{T}}\, \boldsymbol{\Omega}^{\mathrm{T}}\, \boldsymbol{\Psi}^{\mathrm{T}})^{\mathrm{T}}$$

and

$$\mathbf{r} = (\mathbf{r}_\theta^{\mathrm{T}}\, \mathbf{r}_\Omega^{\mathrm{T}}\, \mathbf{r}_\Psi^{\mathrm{T}})^{\mathrm{T}}$$

and $\mathbf{J}$ is the system Jacobian matrix:

$$\mathbf{J} = \frac{\partial \mathbf{r}}{\partial \boldsymbol{\zeta}^{\mathrm{T}}}$$

In practice we interchange the ordering in the $\boldsymbol{\zeta}$ and $\mathbf{r}$ vectors so that $\mathbf{J}$ consists of 3×3 blocks each referring to a particular pair of nodes. For a node i which is not on the boundary the general block J_{ij} is

$$J_{ij} = \begin{pmatrix} K_{ij} + A_{ij}(\boldsymbol{\Psi}) & 0 & -A_{ij}(\boldsymbol{\theta}) \\ -PRC_{ij} & PK_{ij} + A_{ij}(\boldsymbol{\Psi}) & -A_{ij}(\boldsymbol{\Omega}) \\ 0 & -M_{ij} & K_{ij} \end{pmatrix} \tag{13}$$

where

$$A_{ij}(\boldsymbol{\Phi}) = \langle \alpha_i, (\boldsymbol{\partial}_{\mathbf{y}}\boldsymbol{\alpha}^{\mathrm{T}}\boldsymbol{\Phi}, \partial_x\alpha_j - \boldsymbol{\partial}_{\mathbf{x}}\boldsymbol{\alpha}^{\mathrm{T}}\boldsymbol{\Phi}, \partial_y\alpha_j) \rangle \tag{14}$$

The residuals can be conveniently found by multiplying a matrix consisting of the (1, 1), (2, 1), (2, 2), (3, 2) and (3, 3) elements of each J_{ij} block times the current $\boldsymbol{\zeta}$ vector.

Where constant value boundary conditions apply and the residual is defined by (11) the Jacobian matrix row is unit diagonal. Where specified gradient conditions apply the appropriate Jacobian rows are unaffected, except that of course the above described displacement must be applied. Thus for a node i on e.g. an adiabatic, impermeable, and rigid section of boundary the Jacobian matrix block J_{ij} becomes

$$J_{ij} = \begin{pmatrix} K_{ij} + A_{ij}(\Psi) & 0 & -A_{ij}(\boldsymbol{\theta}) \\ 0 & M_{ij} & -K_{ij} \\ 0 & 0 & \delta_{ij} \end{pmatrix} \tag{15}$$

This completes the formulation for the Newton–Raphson method, but one further point should perhaps be considered. Since only two of equations (8) are non-linear, in principle only a 2×2 Jacobian should be needed rather than a 3×3 system. Equation (8c) can be used to substitute for either $\boldsymbol{\Omega}$ or $\boldsymbol{\Psi}$ in (8a) and (8b). If for example the $\mathbf{r}$ and $\boldsymbol{\zeta}$ vectors are reduced to

$$\mathbf{r} = (\mathbf{r}_\theta^{\mathrm{T}}\, \mathbf{r}_\Omega^{\mathrm{T}})^{\mathrm{T}}$$

and

$$\boldsymbol{\zeta} = (\boldsymbol{\theta}\ \boldsymbol{\Psi})^{\mathrm{T}}$$

then the Jacobian is reduced to

$$\begin{pmatrix} \mathbf{K}+\mathbf{A}(\boldsymbol{\Psi}) & -\mathbf{A}(\boldsymbol{\theta}) \\ -PR\mathbf{C} & -\mathbf{A}(\boldsymbol{\Omega})+(P\mathbf{K}+\mathbf{A}(\boldsymbol{\Psi}))\mathbf{M}^{-1}\mathbf{K} \end{pmatrix}$$

with the subsidiary relation

$$\boldsymbol{\Omega} = \mathbf{M}^{-1}\mathbf{K}\boldsymbol{\Psi}$$

used at each iteration. However we now have the triple products $\mathbf{K}\mathbf{M}^{-1}\mathbf{K}$ and $\mathbf{A}_1(\Psi)\mathbf{M}^{-1}\mathbf{K}$. In forming these there will presumably be considerable fill-in, requiring substantial additional Jacobian blocks. This approach therefore would seem to be unlikely to lead to any advantage.

3. FIRST ATTEMPTS: SEGREGATED APPROACHES AND BOUNDARY FORMULAE

At first, following Tabarrok and Lin,[15] attempts were made to achieve a steady state solution by converting (8) to three Poisson equations:

$$\mathbf{K}\boldsymbol{\theta} = -\mathbf{a}(\bar{\boldsymbol{\Psi}}, \bar{\boldsymbol{\theta}}) + \mathbf{b}(\theta_n) \tag{16a}$$

$$P\mathbf{K}\boldsymbol{\Omega} = -\mathbf{a}(\bar{\boldsymbol{\Psi}}, \bar{\boldsymbol{\Omega}}) + PR\mathbf{C}\bar{\boldsymbol{\theta}} + \mathbf{b}(\Omega_n) \tag{16b}$$

$$\mathbf{K}\boldsymbol{\Psi} = \mathbf{M}\bar{\boldsymbol{\Omega}} + \mathbf{b}(\Psi_n) \tag{16c}$$

and attempting to find a solution by iteration. Here each equation is solved in turn for $\boldsymbol{\theta}, \boldsymbol{\Omega}$, and $\boldsymbol{\Psi}$ using right hand sides computed from the last previously determined values denoted by bars over the symbols. The attraction of such an approach is that only a single inverse factorization of one symmetric matrix K need be made, the remaining computing consisting of multiple right hand side formation and multiplications. Further the right hand side formations can be done at element level so that the only major storage required is that for the inverse factors of K. However this approach was found to work only for very low Rayleigh numbers, and under-relaxation of variable values in the loop was found to be necessary to prevent instability. Under-relaxation factors as small as 0·1 or 0·2 were sometimes required. No need for under-relaxation was mentioned by Tabarrok and Lin. For $Ra = 10^4$ some wander in the results could not be eliminated. The iteration form was thus considered to be intrinsically unstable for any Rayleigh number giving significant convection.

To try to ameliorate this instability the next step taken was to incorporate the velocities into the equation matrices, so that (16a) and (16b) become

$$(\mathbf{K}+\mathbf{A}(\bar{\boldsymbol{\Psi}}))\boldsymbol{\theta} = \mathbf{b}(\theta_n) \tag{17a}$$

$$(P\mathbf{K}+\mathbf{A}(\bar{\boldsymbol{\Psi}}))\boldsymbol{\Omega} = PR\mathbf{C}\bar{\boldsymbol{\theta}} + \mathbf{b}(\Omega_n) \tag{17b}$$

The matrices for the solution of (17a) and (17b) must now be re-formed and re-factorized at each iteration (and they are asymmetric). Although there was some improvement in stability over the previous approach, the rate of convergence in terms of computation time was much the same. For $Ra = 10^4$ an under-relaxation factor of 0·3 was still required, and it was not considered worthwhile to try higher Rayleigh numbers.

At this stage, again following Tabarrok and Lin and others, the stream function gradient or no-slip boundary condition was being treated by a boundary vorticity formula method. Apart from the convergence limitation discussed above, there was considerable difficulty with this boundary condition. Before describing this we digress to a discussion of the boundary vorticity methods in general, as they have been widely used.

The methods employ a family of approximate formulae to define vorticity boundary values from the stream function field determined in a previous iteration.[17] The simplest and most commonly used formula is derived by expanding the stream function in a Taylor series along an inward normal from a wall:

$$\psi_1 = \psi_0 + h\frac{\partial\psi}{\partial x}\bigg|_0 + \frac{h^2}{2}\frac{\partial^2\psi}{\partial x^2}\bigg|_0 + \frac{h^3}{6}\frac{\partial^3\psi}{\partial x^3}\bigg|_0 + \ldots$$

Where subscript 0 indicates the point on the wall and subscript 1 indicates an interior point. Using the no-slip condition on the wall

$$\frac{\partial\psi}{\partial x}\bigg|_0 = 0$$

and the constancy of ψ along the wall which gives

$$\frac{\partial^2\psi}{\partial x^2}\bigg|_0 = \nabla^2\psi|_0 = -\omega_0$$

we have

$$\omega_0 = -\frac{2}{h^2}(\psi_1 - \psi_0) - \frac{h}{3}\frac{\partial^3\psi}{\partial x^3}\bigg|_0 \ldots \tag{18}$$

The formula is obtained by truncating (18) after the first term on the right hand side. More elaborate formulae, in which the error is reduced by one order by employing two internal values of stream function or one value of stream function and one of vorticity, have also been used. The formulae are commonly used with what are termed 'second order' finite differences, i.e. finite difference formulae for which the error is second order in h. These formulae correspond to what are termed 'first order' finite elements, i.e. linear interpolation. From a finite element viewpoint it is evident that in the solution of these formulae for stream function, the value of ψ_1 will have been determined on the basis that ψ varies linearly between ψ_0 and ψ_1. To define a boundary vorticity by drawing a pure quadratic to ψ_1 then seems artificial and likely to lead to error. To make the point more clearly, it is evident that the boundary vorticity value obtained is strongly dependent on the point on the linear variation to which the quadratic is drawn. Remembering that perfect satisfaction of the boundary conditions requires the linear variation to have a slope of zero makes the procedure seem to have even less sense. Such a procedure would seem to be approximately valid with linear elements (or the corresponding finite difference formulae) only if the quadratic extends over a number of elements (or finite difference points), in which case of course the error of first order in h in (18) will be enhanced.

What finite element work there has been using the stream function–vorticity approach has used formula (18) or a similar one. The early work of Cheng[6] on flow in pipes used this formula with first order elements as did Tabarrok and Lin. Baker[7] used the more elaborate formula which employs an internal vorticity value, but again apparently mainly with first order elements. (Baker also used second order elements; we discuss these next).

For the attempts at solution with the methods of equations (16) and (17) the above simple formula was used to define boundary vorticities, but with second order elements instead of the first order elements used by Tabarrok and Lin. However it was found that boundary slip velocities were very large: up to 50 per cent of mean velocities for $Ra = 10^3$ and worse for $Ra = 10^4$, and clearly the boundary condition was not being satisfied at all. The reason is that the solution for ψ obtained from (16c) in an element adjacent to the boundary results from Ω throughout this element. In a second order element only a constant value of $\partial^2\psi/\partial n^2$ is allowed along a normal. The value obtained for this in the solution of (16c) corresponds to some average of Ω along the normal after allowance is made for the second derivative in the perpendicular direction. To feed this value back as wall vorticity will lead to gradual progression from the true solution, particularly as the most rapid variation of vorticity in the problem occurs adjacent to the wall. Presumably if the order of element used were increased the error would gradually diminish. No improvement would be expected from changing to the more elaborate wall formulae on the other hand as long as the order of element remains the same.

Finally with these approaches an attempt was made to satisfy the gradient condition iteratively. Since increases in both first and second derivatives of stream function at the wall change internal values in the same direction, it is possible to guess at a change of boundary vorticity used in the input to the solution of (16b) or (17b) to give a certain change of stream function boundary gradient in the following solution of equation (16c). With under-relaxation and sufficient iteration, it was found to be possible to bring the boundary slip velocities down to around 5 per cent of the mean velocity. However, this is not an easy method of achieving a solution because there are now two nested iteration loops which tend to interact to make convergence difficult unless the inner loop is allowed to fully converge at each step of the outer loop. Also there remained a slight wander at $Ra = 10^4$ which discouraged any attempts at higher Rayleigh numbers.

In contrast to the results of these approaches, the Newton–Raphson method, as outlined in the previous section, was found to work very well, as described in the next sections.

4. SOLUTION IMPLEMENTATION

All the results given in this paper were obtained with the Newton–Raphson method as outlined in Section 2. An isoparametric program package MANFEP[18] was used as a computational basis. This provides triangular Lagrangian elements with from first to fourth order interpolation, and in-core solution by the Zollenkopf[19] sparse matrix method. The latter involves a 'near-optimal' elimination sequence (selection based on minimum branches), separate simulation, reduction, and factor multiplication stages, and linked-list matrix element storage. For this work the solution routines were adapted to provide block sparse processing, i.e. each node–node block of 3×3 elements is stored and processed contiguously, and the linked-list indexing applies to the blocks rather than the elements. For each problem mesh the simulation step needs to be performed only once, i.e. it is not repeated for each Newton–Raphson iteration. The solution processing was performed in single precision (i.e. 4 bytes per number).

For Rayleigh numbers of 10^3, 10^4 and 10^5 in the square cavity problem of the next section, a solution could be obtained starting from scratch, i.e. all variables zero except for the boundary fixed temperatures. For the first two of these Rayleigh numbers, this took 4 or 5 Newton–Raphson iterations. For the Rayleigh numbers of 10^5, 10^6 and 10^7, solutions were usually obtained starting from the Rayleigh number one factor of 10 smaller, and this again

took 4 or 5 iterations. Convergence in practice meant that the residuals were brought to zero to machine precision: convergence is extremely rapid close to the solution. Convergence at the highest Rayleigh numbers and small Prandtl numbers is discussed further in the next section.

For a third order, 72 triangular element, 19×19 total nodes, problem, computing time was 8 seconds per iteration on an IBM 360–195. When communication to this machine broke down, computing was continued on a Prime 400 multi-user minicomputer with 384 K bytes real store and a virtual system with a 128 K byte addressing space. Because of the limited page size it was found to be essential to rearrange the storage. The Zollenkopf 'near-optimal' elimination sequence was replaced by a frontal sequence and storage was rearranged so that blocks in processed block rows/columns were stored adjacently and in processing sequence. Thus, while still programmed as an 'in-core' solution, the virtual system automatically produces some of the effect of a frontal method where matrix factors are written to disk. Time per iteration on the Prime was $7\frac{1}{2}$ minutes, about twice as great as expected from the usual ratio of speeds of the machines, 25, on account of the extra fill-in of the frontal sequence, and the lower efficiency of the Prime for large programs. Maximum virtual store used for matrix storage was about 750 K bytes for the 28×19 mesh. The upper limit on total program store available on the Prime, 1 M byte, was not reached with the meshes reported on in the next section but clearly little expansion would be possible without converting to a fully frontal method.

4. RESULTS AND DISCUSSION

Results have been obtained for the problem of a square cavity with isothermal vertical walls at different temperatures and horizontal adiabatic walls. This problem has been proposed by de Vahl Dvis *et al.*[16] as a standard for comparing different numerical methods for fluid flow and convection. For all the computations a rectangular mesh was generated from a set of x co-ordinates and a set of y co-ordinates and each rectangle divided into two triangular elements. The co-ordinate sets however were varied according to the nature of the solution expected. First results were obtained for air, $Pr = 0{\cdot}71$, and a range of Rayleigh numbers.

At the outset it was assumed that at least second order interpolation would be necessary, since with first order interpolation the two boundary conditions on stream function would require the stream function to be zero throughout the elements adjacent to the boundary. Starting with the lowest Rayleigh number of 10^3, computations were made with second, third, and fourth order interpolation. The results for Nusselt number shown in Table I suggest that at least third order interpolation should be used.

In the sequence of powers of 10 in Rayleigh number, the value of 10^4 is that for which there is substantial convection in relation to conduction, i.e. all terms of the equations are having effect, but yet the action if fairly distributed over the volume of the enclosure. For lower numbers heat transfer is conduction dominated, while for higher numbers the action is concentrated close to the boundaries. Therefore this is the most useful Rayleigh number at which to examine the effect of variation of mesh size. Results are shown in Table II. Generally the meshes were made somewhat finer towards the boundaries. As seen, quite good results were obtained for quite coarse meshes. The table also demonstrates the desirability of having somewhat more nodes in the horizontal direction than in the vertical direction. It is noticeable that the Nusselt numbers exhibit a progressive shift with increasing mesh refinement whereas the central stream function values seem to fluctuate randomly within a constant range.

Table I. Mean Nusselt number for $Ra = 10^3$, $Pr = 0{\cdot}71$, and different approximation orders and meshes. For each mesh total number of nodes is given in each direction; nodes are equally spaced except for mesh marked *, for which internal primary node co-ordinates are 0·1, 0·3, 0·5, 0·7, 0·9. In all cases central stream function value, $\psi_c = -1{\cdot}17$

Order	Mesh	$\overline{Nu}$
2	13×13	1·125
2	19×19	1·120
3	13×13	1·1136
3	19×19	1·1155
3	19×19*	1·1165
4	17×17	1·1160
4	21×21	1·1162

By contrast to the effect of change of mesh size, the change from third to second order interpolation for the same number of total nodes shows a much larger change in Nusselt number (last line of Table II). This confirms the suggestion of the results for $Ra = 10^3$ that at least third order interpolation should be used. This is understandable in terms of the degree to which equation (3c) can be satisfied: while at least second order interpolation for stream function is required to give acceptable satisfaction of this equation within an element for any non-zero vorticity, at least third order interpolation is required if the vorticity varies rapidly, which is particularly the case near a hot or cold wall in this problem. All further computations in this work were made with third order interpolation.

For the higher Rayleigh numbers of 10^5, 10^6, and 10^7, results for the quantities of principal physical interest are shown in Table III. An idea of the sensitivity of these results to

Table II. Central stream function, ψ_c, and mean Nusselt number, $\overline{Nu}$, for $Ra = 10^4$, $Pr = 0{\cdot}71$. Total number of nodes given in horizontal × vertical directions. 28×19 meshes are those on lines 2 to 4 of Table IV

Order	Mesh	ψ_c	$\overline{Nu}$
3	13×10	−5·085	2·217
3	13×13	−5·062	2·222
3	16×13	−5·086	2·225
3	16×16	−5·087	2·227
3	19×16	−5·077	2·231
3	19×19	−5·074	2·232
3	22×16	−5·084	2·237
3	22×19	−5·081	2·238
3	28×19−(2)	−5·075	2·241
3	28×19−(3)	−5·081	2·241
3	28×19−(4)	−5·091	2·242
2	19×19	−5·07	2·310

Table III. Central and minimum stream function values, ψ_c and ψ_m, location of minimum, mean Nusselt number, and maximum vertical velocity on the horizontal mid-line and its distance from the vertical wall, for air ($Pr = 0{\cdot}71$) and range of Rayleigh numbers. Meshes 22×19 for $Ra = 10^5$ and 10^6; 28×19 (line 6, Table IV) for $Ra = 10^7$

Ra	ψ_c	ψ_m at (x, y)	$\overline{Nu}$	V_y	x
10^5	−9·10	−9·64 (0·28, 0·60)	4·50	70·0	0·05–0·07
10^6	−16·4	−16·9 (0·14, 0·55)	8·77	222	0·037
10^7	−29·3	−30·3 (0·08, 0·57)	16·5	710	0·022

mesh fineness and to the concentration of mesh fineness in different regions is given in Table IV. For example, in comparison with the mesh of line 1, that of line 2 has a closer distribution of x co-ordinates over the main region, while that of line 4 has a finer distribution close to the isothermal walls. For $Ra = 10^5$, the peak in vertical velocity distribution on the horizontal mid-line is sufficiently broad that the location of the maximum is somewhat mesh dependent although the value is essentially unchanged, as shown in Table III.

For $Ra = 10^7$ it was found to be essential to have the width of the elements adjacent to the isothermal walls no greater than 0·03, and thus comparisons could only be made amongst meshes of 28×19 nodes with the present in-core solution program and computer. Within this limitation the results were all consistent with those given in Table III.

Table V compares the results with those given in Table I of Reference 20 in the cases where the Rayleigh numbers are the same. Curiously, for $Ra = 10^6$, the present results are in accord with those of Mallinson and de Vahl Davis on maximum stream function value but not on Nusselt number, while comparing with the results of Jones the situation is the other way round. Again for $Ra = 10^4$, the agreement with Jones is excellent for Nusselt number but not quite so good for stream function. Note that the discrepancy in the latter values is larger than the variation shown in Table II.

Contour plots for temperature, stream function and vorticity for these parameter values are shown in Figure 1. The vorticity plots generally show a cental negative area (rotation in the direction of the main circulation) separated by a zero contour from positive vorticity regions adjacent to the walls. By $Ra = 10^4$ there are two distinct valleys of vorticity in the central area; with increasing Ra these move apart leaving a central area with little action. By $Ra = 10^5$ a positive vorticity area (rotation against the main circulation) has appeared in this central area on each side. This presumably is created, on the cold side for example, by the viscous action of the reflected updraught on the interior side of the wall downdraught. The further islands of positive vorticity that appear for $Ra = 10^7$ are of sufficiently small vorticity

Table IV. Illustration of sensitivity to mesh grading for $Pr = 0{\cdot}71$ and $Ra = 10^5$ and 10^6. Co-ordinates given are those of the internal primary nodes (i.e. triangle vertices) within half of the cavity

	Total nodes ($x \times y$)	x-co-ordinates	y-co-ordinates	$Ra = 10^5$ ψ_c	ψ_m	$\overline{Nu}$	$Ra = 10^6$ ψ_c	ψ_m	$\overline{Nu}$
1	22×19	0·05, 0·15, 0·32	0·1, 0·3, 0·5	−9·103	−9·642	4·497	−16·43	−16·87	8·774
2	28×19	0·05, 0·15, 0·25, 0·40	0·1, 0·3, 0·5	−9·112	−9·626	4·497	−16·38	−16·85	8·773
3	28×19	0·05, 0·12, 0·20, 0·35	0·1, 0·3, 0·5	−9·106	−9·630	4·498	−16·40	−16·81	8·772
4	28×19	0·03, 0·07, 0·15, 0·32	0·1, 0·3, 0·5	−9·102	−9·641	4·512	−16·44	−16·84	8·769
5	28×19	0·03, 0·07, 0·15, 0·32	0·07, 0·25, 0·5	−9·092	−9·657	4·511	−16·51	−16·85	8·767
6	28×19	0·03, 0·08, 0·18, 0·35	0·06, 0·2, 0·5	Used for $Ra = 10^7$: Table III					

Table V. Comparison of stream function and Nusselt number values with those of Jones and Mallinson and De Vahl Davis. Meshes (1) and (2) are those of lines 1 and 2 of Table IV

Ra		Mesh	ψ_c	ψ_m	$\overline{Nu}$
10^4	This work	$28\times19-(2)$	5·08		2·241
	Jones	45×45	5·15		2·242
10^6	This work	$22\times19-(1)$	16·4	16·9	8·77
	Jones	45×45	17·6	18·1	8·77
	M. and De V. D.	51×51		17·1	8·12

magnitude (order of 200) that they probably do not represent real positive circulation regions, i.e. their appearance really means that the vorticity is essentially zero over the interior region.

The solution for $Ra = 10^7$ was obtained by starting from the solution for $Ra = 10^6$. Starting from the $Ra = 10^7$ solution, a solution for $Ra = 10^8$ was not obtainable; the highest Rayleigh number for which a solution was obtained was 2×10^7. An attempt to achieve a solution for $Ra = 5\times10^7$ starting from the $Ra = 2\times10^7$ solution did not converge. However, it was felt that solutions for slightly higher Rayleigh numbers could probably be obtained if the change in Ra were divided into smaller steps or if other means, e.g. an incremental method, were adopted.

It is assumed that the limit on the ability to obtain a solution arises from the closeness of the transition to the turbulent regime. An attempt to take a large step in Rayleigh number near this boundary may take the variables across the boundary in the iteration process at which point of course convergence will be lost. Experimentally turbulence is found to set in when the Rayleigh number is in the region of 10^8.[21,22]

The final investigation made was sensitivity to variation of Prandtl number. Generally solutions were sought for Prandtl numbers of 10^{-2} and 10^2 using solutions for the same Rayleigh number and $Pr = 0{\cdot}71$ for starting values. We discuss first the physical results obtained and then the question of limits to the ability to obtain a solution.

Table VI shows the results. In comparing results for different Prandtl numbers it should be remembered that the stream function and velocity values are defined on the thermal diffusivity time scale, equation (1). The corresponding values measured on the viscous time scale are obtained by dividing by the Prandtl number (equation (5)). However the results indicate that the choice of thermal time scale and Rayleigh and Prandtl numbers as independent parameters is the most appropriate for classifying the results. The principle dependence is then on Rayleigh number. Further the position of the maximum in the profile of vertical velocity on the horizontal mid-line, which is independent of choice of non-dimensionalization, is seen to depend to an extent on Rayleigh number alone.

However the situation is different when it comes to considering the boundary between laminar and turbulent regimes. We assume that this boundary or the closeness of it provides the only limit to the ability to obtain a solution. Since it is the transport of momentum, not thermal energy, which governs the physical stability limit, it is the viscous time scale which is relevant for this question. When the two velocity-determining equations are written with the viscous time scale non-dimensionalization, equations (6b) and (6c), the only parameter to enter is seen to be the Grashoff number, the parameter which is independent of the thermal diffusivity, in the temperature gradient 'driving' term. Thus for a fixed temperature field a reduction in Prandtl number has the same effect as an increase in Rayleigh number.

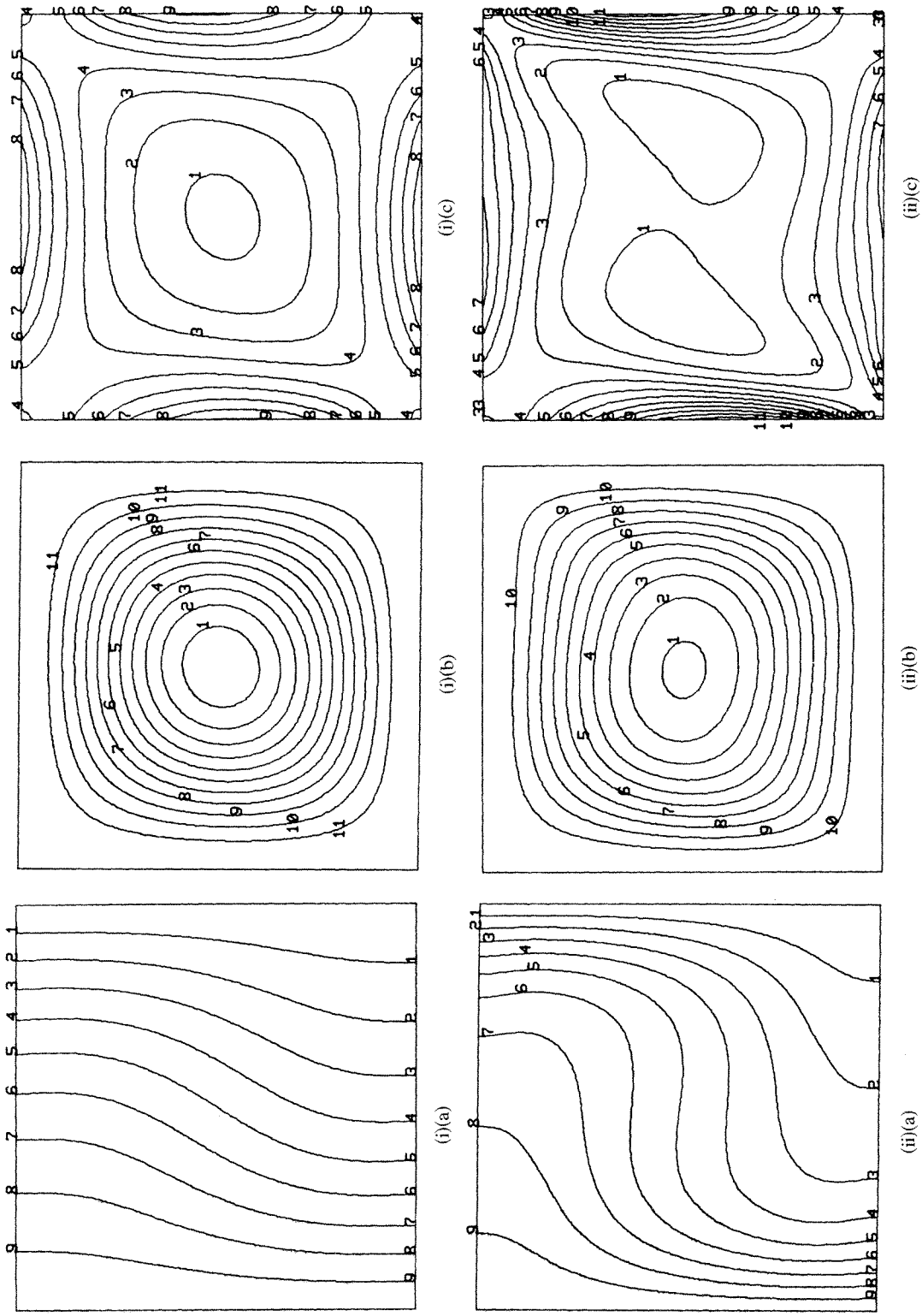

Figure 1. For key see p. 363

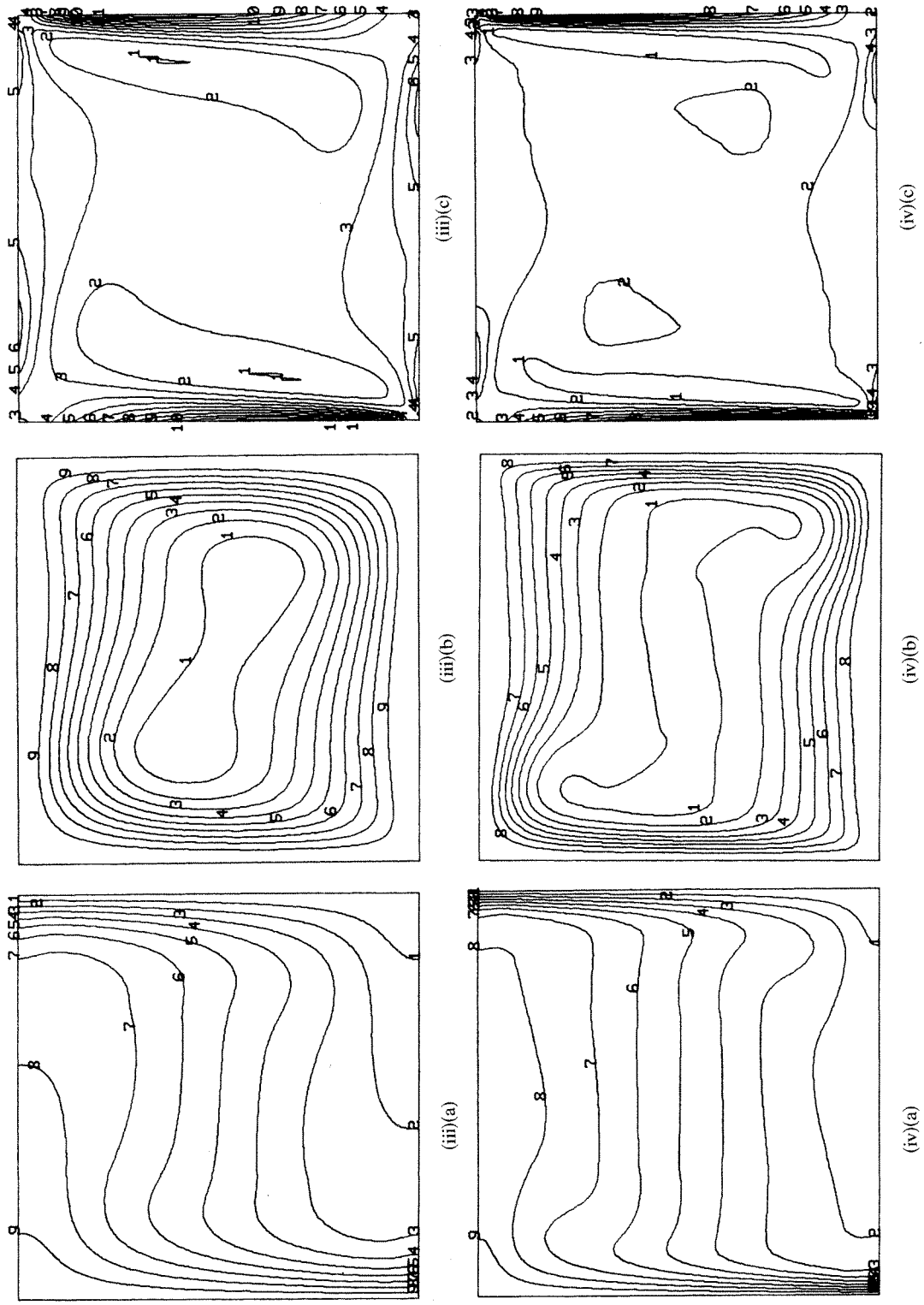
(iii)(a)
(iii)(b)
(iii)(c)
(iv)(a)
(iv)(b)
(iv)(c)

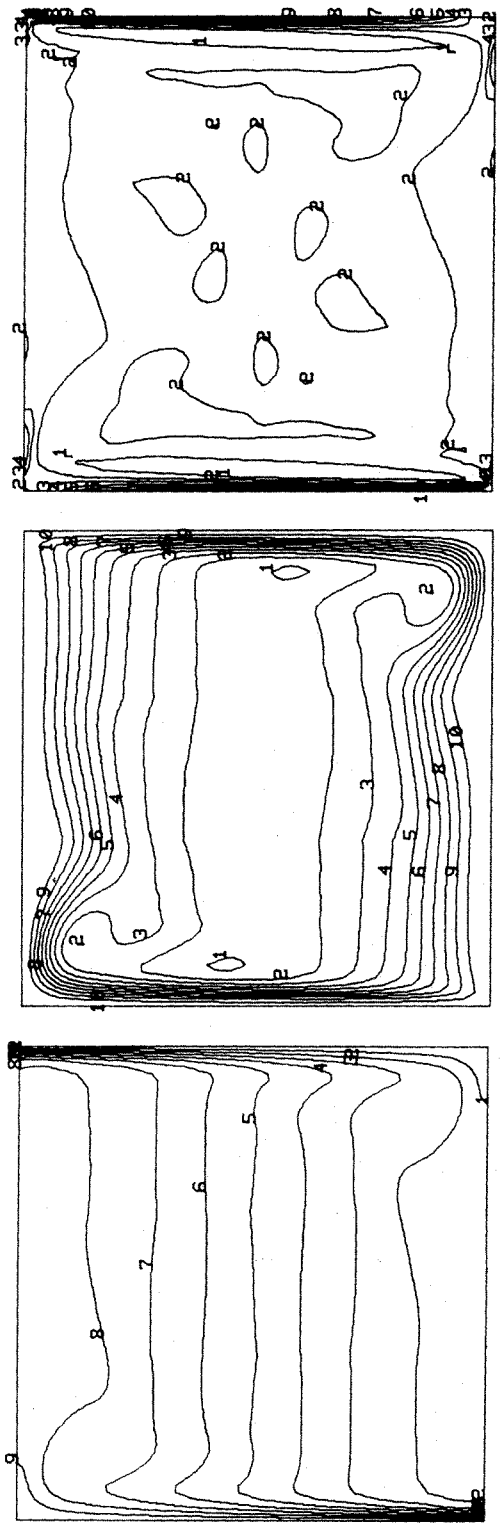

(v)(a) (v)(b) (v)(c)

Figure 1. Contour plots for temperature, stream function, and vorticity for $Pr = 0{\cdot}71$.
(i) $Ra = 10^3$
(ii) $Ra = 10^4$
(iii) $Ra = 10^5$
(iv) $Ra = 10^6$
(v) $Ra = 10^7$
(a) Temperature, in all cases contour values are 0·1, (intervals of 0·1), to 0·9.
(b) Streamlines, values are
(i) −1·1, (0·1), −0·1
(ii) −5·0, (0·5), −0·5
(ii) −9·0, (1·0), −1·0
(iv) −16, (2), −2
(v) −30, (3), −3
(c) Vorticity, contour values are
(i) −30, (10), 50 (contour 4 is zero)
(ii) −100, (50), 400 (contour 3 is zero)
(iii) −600, (300), 2400 (contour 3 is zero)
(iv) -2×10^3, (2×10^3), 14×10^3 (contour 2 is zero)
(v) -10×10^3, (10×10^3), 80×10^3 (contour 2 is zero)

Table VI. Comparison of results for different Prandtl numbers. Third set of columns is maximum vertical velocity on the horizontal mid-line, and its distance from the wall

		Nu			ψ_c			V_y at (x)	
Ra	Pr	10^{-2}	0·71	10^2	10^{-2}	0·71	10^2	10^{-2}	0·71	10^2
10^4		1·957	2·241	2·27	−4·65	−5·08	−5·18	15·2 (0·15)	19·8 (0·12)	19·8 (0·12)
10^5		3·25	4·50	4·69	−7·19	−9·11	−10·9	41·6 (0·08)	70·6 (0·07)	73·1 (0·07)
10^6			8·77	9·17		−16·4	−18·7		222 (0·037)	246 (0·05)
10^7			16·5			−29·2			710 (0·022)	

In accordance with this consideration it was found that the Grashoff number alone was indeed a rough guide to the limit to the ability to obtain solutions. Since however we are dealing with a coupled problem, not a fixed temperature field, a closer examination needs to be made. Comparing the results in Table VI for $Ra = 10^5, Pr = 10^{-2}$ with those for $Ra = 10^7, Pr = 0{\cdot}71$, when the velocity values shown are converted to the viscous-based non-dimensionalization they become 4160 and 1000, respectively. These values might also be called local Reynolds numbers. Presumably these values are representative of the relative scale of the two velocity fields as a whole, so that the first case is closer to the boundary of the turbulent regime than the second. The relative ease of obtaining the two solutions was found to be in accord with this: the solution for $Ra = 10^7, Pr = 0{\cdot}71$ was obtained from the solution for $Ra = 10^6, Pr = 0{\cdot}71$ in a single step, but to obtain a solution for $Ra = 10^5, Pr = 10^{-2}$ required an intermediate solution at $Ra = 10^5, Pr = 3 \times 10^{-2}$.

It might be worth adding that in Olsen and Tuann's study[9] of the driven cavity problem, the greatest Reynolds number (defined by the velocity of the moving wall) for which solutions were readily obtained (3450) was of the same order as the greater Reynolds number quoted above.

Needless to say, no difficulties were experienced in obtaining solutions for $Pr = 10^2$ from those at $Pr = 0{\cdot}71$ and the same Rayleigh number. The results for $Pr = 10^2$ in Table VI suggest that for sufficiently high Pr the solution converges to a constant one. This is understandable in terms of equations (3) with left hand sides of zero, since sufficiently large Pr will be equivalent to neglect of the advective term of (3b) and change of Pr has no other effect on the system.

6. CONCLUSIONS

The stream function–vorticity approach to 2-dimensional incompressible viscous flow and convection has been found to work well provided that certain conditions are satisfied. First, the two boundary conditions for stream function must be applied directly, not through defining vorticity boundary values by approximate formulae employed iteratively. Direct application of the boundary conditions can be achieved by the finite element discretization and application of a displacement of the appropriate discrete equations. Second, the order of interpolation must be sufficient to allow both boundary conditions to be satisfied and still allow a measure of freedom in elements adjacent to the boundary. Finally, steady state solutions can rapidly be achieved by a fully coupled simultaneous procedure (i.e. treating all variables as simultaneous unknowns) using the Newton–Raphson method. Solution procedures in which values for each variable are updated by solution of each equation in turn were not found to be successful.

With the above conditions results have been obtained for a wide range of the two

independent parameters of the natural convection problem. The limits of the ability of the formulation to produce a steady state solution under variation of these two parameters were entirely consistent with the following assumption: that the method will always produce the solution when the flow is physically steady, but will not give a steady solution when the flow is physically unsteady. There are numerical methods that differ on the second of these criteria, as well as those that differ on the first. In particular it must be pointed out that with the present method there is no need for upwind differencing, asymmetric basis functions, or exponential interpolation, etc.

For two dimensional problems the formulation has a measure of economy over the primitive variables approach which has been adopted by most finite element workers, as well as having the advantage of satisfying continuity exactly. A quantitative comparison with the fourth order equation method of Olson and Tuann[9] would be of interest. Two avenues for improvement of the present method would be towards employing Hermitian elements (i.e. derivatives as well as variable values continuous between elements), and towards use of an automatic mesh adjustment algorithm whereby the mesh is modified according to the solution found in the iteration process. The latter would be particularly valuable for the middle and higher Rayleigh numbers where the action is very unevenly distributed.

Comparison of results with those of two finite difference workers using finer meshes show some differences. It is suggested that the differences probably arise from the different treatment of the boundary conditions.

More detailed conclusions are as follows. The practice of iteratively defining boundary vorticity from the stream function field along the boundary normal is viewed as likely to lead to considerable error. It should be noted that the method of direct application of boundary conditions employed here can be used with segregated solution procedures as well as simultaneous ones, since it requires only movement of discrete equations after the finite element discretization has been applied.

The impermeable, or fixed stream function, boundary condition is effectively satisfied exactly in the formulation, but the no-slip or normal gradient condition is only satisfied as part of the approximation. The boundary slip velocities in obtained solutions can of course be examined, and these give a very useful idea of the adequacy of the local mesh fineness.

Third order elements were used for the work reported here. For stream function this has some equivalence to the second order interpolation for velocity commonly used in primitive variable approaches, although of course the equivalence stops there.

Extension to more general geometries from the square cavity modelled here is obviously straightforward with the isoparametric finite element method. However the program used here needs modifying to full frontal solution for much larger problems.

ACKNOWLEDGEMENTS

The author is indebted to Brush Switchgear Ltd. and the United Kingdom Science Research Council for support during different parts of the time during which this work was done. He would like to thank Dr. P. Johns for making this possible and for his interest in the work.

REFERENCES

1. C. Taylor and P. Hood, 'A numerical solution of the Navier–Stokes equations using the finite element technique', *Computers and Fluids*, **1**, 73–100 (1973).
2. P. Hood and C. Taylor, 'Navier–Stokes equations using mixed interpolation', *Proc. Int. Symp. Finite element methods in flow problems*, Swansea, 121–132 (1974).

3. J. T. Oden and L. C. Wellford, 'Analysis of flow of viscous fluids by the finite element method', *AIAA Journal*, **10,** 1590–1599 (1972).
4. M. Kawahara, N. Yoshimura, K. Nakagawa and H. Ohsaka, 'Steady and unsteady finite element analysis of incompressible viscous fluid', *Int. J. Num. Meth. Eng.*, **10,** 437–456 (1976).
5. D. K. Gartling and E. B. Becker, 'Finite element analysis of viscous incompressible fluid flow', *Comp. Methods App. Mech. Engng.*, **8,** 51–60 and 127–138 (1976).
6. R. T. Cheng, 'Numerical solution of the Navier–Stokes equations by the finite element method', *Physica of Fluids*, **15,** 2098–2105 (1972).
7. A. J. Baker, 'Finite element solution algorithm for viscous incompressible fluid dynamics', *Int. J. Num. Meth. Eng.*, **6,** 89–101 (1973).
8. A. Campion-Renson and M. J. Crochet, 'On the stream function–vorticity finite element solutions of Navier–Stokes equations', *Int. J. Num. Meth. Eng.*, **12,** 1809–1818 (1978).
9. M. D. Olsen and S. Y. Tuann, 'New finite element results for the square cavity', *Computers and Fluids*, **7,** 123–135 (1979).
10. D. K. Gartling, 'Convective heat transfer analysis by the finite element method', *Comp. Methods Appl. Mechs. Engng.*, **12,** 365–382 (1977).
11. C. Taylor and A. Z. Ijam, 'A finite element numerical solution of natural convection in enclosed cavities', *Comp. Methods App. Mechs. Engng.*, **19,** 429–446 (1979).
12. D. L. Young, J. A. Liggett and R. H. Gallagher, 'Steady stratified circulation in a cavity', *J. Am. Soc. Civil Engrs.*, EMI, **102,** 1–17 (1976).
13. R. Piva and A. DiCarlo, 'Numerical techniques for convection/diffusion problems', *Proc. Conf. Mathematics of Finite Elements and Applications*, 399–409 (1970).
14. O. C. Zienkiewicz, R. H. Gallagher and P. Hood, Newtonian and non-Newtonian viscous incompressible flow. Temperature induced flows. Finite element solutions', *Proc. Conf. Mathematics of Finite Elements and Applications*, 235–267 (1976).
15. B. Tabarrok and R. C. Lin, 'Finite element analysis of free convection flows', *Int. J. Heat Mass Transfer*, **20,** 953–960 (1977).
16. G. de Vahl Davis, I. P. Jones and P. J. Roache, 'Natural convection in an enclosed cavity: a comparison problem', General announcement, e.g. *Computers and Fluids*, **7,** 315–316 (1979).
17. P. J. Roache, *Computational Fluid Dynamics*, revised printing, Hermosa Press, Albuquerque, NM, USA, 1976, pp. 139–146.
18. TASC Ltd., 163 McAdam Ave., Winnipeg, Manitoba, R2W OA7, Canada.
19. K. Zollenkopf, 'Bifactorization: basic computational algorithm and programming techniques', in *Large Sparse Sets of Linear Equations*, ed. J. K. Reid, Academic Press, NY, 1971, pp. 75–96.
20. I. P. Jones, 'A comparison problem for numerical methods in fluid dynamics, the "double glazing" problem', in *Numerical Methods in Thermal Problems*, Proc. 1st Conf., Swansea, July 1979, Pineridge Press, Swansea, UK, pp. 338–348.
21. J. W. W. Elder, 'Laminar free convection in a vertical slot', *J. Fluid Mech.*, **23,** 77–98 (1965).
22. J. W. Elder, 'Turbulent free convection in a vertical slot', *J. Fluid Mech.* **23,** 99–111 (1965).